5094 *Inorg. Chem.* **2010**, *49*, 5094–5100
DOI: 10.1021/ic1002429

Inorganic Chemistry
Article

Synthesis, Structures, and Electroluminescent Properties of Scandium N,O-Chelated Complexes toward Near-White Organic Light-Emitting Diodes

Marina A. Katkova, Tatyana V. Balashova, Vasilii A. Ilichev, Alexey N. Konev, Nikolai A. Isachenkov, Georgy K. Fukin, Sergey Yu. Ketkov, and Mikhail N. Bochkarev*

G.A. Razuvaev Institute of Organometallic Chemistry of RAS, Tropinina 49, Nizhny Novgorod, 603950, Russia

Received February 5, 2010

Three members of a new class of electroluminescent, neutral, and monomeric scandium N,O-chelate complexes, namely, Sc(III)-tris-2-(2-benzoimidazol-2-yl)phenolate (**1**), Sc(III)-tris-2-(2-benzoxyazol-2-yl)phenolate (**2**), and Sc(III)-tris-2-(2-benzothiazol-2-yl)phenolate (**3**), have been prepared and X-ray characterized. DFT calculations have been performed. In contrast to the most frequently applied dual or multiple dopants in multilayer white OLED devices, all our simpler devices with the configuration of indium tin oxide/N,N′-bis(3-methylphenyl)-N,N′-diphenylbenzidine/neat scandium complex/Yb exhibit close to near-white emission with a blue hue ($CIE_{x,y}$ = 0.2147, 0.2379) in the case of **1**, a cyan hue (0.2702, 0.3524) in the case of **2**, and a yellowish hue (0.3468; 0.4284) in the case of **3**.

Introduction

Recently, a good deal of attention has been paid to the application of metal complexes as electroluminescent materials for organic light emitting diodes (OLED).[1] Many research groups have focused on the preparation of efficient light-emitting compounds based on known classes of main-group, transition-metal, and lanthanide coordination complexes.[2] Neutral coordination complexes have shown an excellent light-emitting nature and sublimation properties under vacuum conditions. Despite the large number of scandium complexes reported in the chemical literature, their electroluminescent properties remain comparatively unexplored.[3] Recently, we have found, unlike in previous studies,[4] that the electroluminescent properties of scandium 8-quinolinolate complex Scq_3 surpass the properties of standard Alq_3.[5] These data gave us the grounds to consider scandium metal−organic complexes as promising material for the design of efficient OLEDs. The aim of this work was the synthesis of new air-stable volatile scandium complexes with heterocyclic 2-(2-benzoimidazol-2-yl)phenolate, 2-(2-benzoxyazol-2-yl)phenolate, and 2-(2-benzothiazol-2-yl)phenolate ligands and their investigation as emissive materials in OLED. Herein, we prepared devices consisting of exclusively vacuum deposited layers using ITO glass as the anode, N,N′-bis(3-methylphenyl)-N,N′-diphenylbenzidine (TPD) as the hole-transporting layer, the scandium heterocyclic complexes as the neat emission/electron-transport layers, and Yb as the cathode. It should be noted that a close to near-white EL has been achieved in this work using a neat emissive layer in contrast to the most frequently applied dual or multiple dopants in multilayer white OLED devices.

Experimental Section

General Procedures. All manipulations were carried under a vacuum using standard Schlenk techniques. The scandium complex $Sc[N(SiMe_3)_2]_3$ was synthesized according to the published procedure.[6] 2-(2-Hyodroxyphenyl)-1H-benzimidazole, 2-(2-hydroxyphenyl)benzoxazole, and 2-(2-hydroxyphenyl)-benzothiazole were purchased from Aldrich. Scandium metal analyses were carried out by complexometric titration. The C, H, and N elemental analyses were performed by the Microanalytical Laboratory of IOMC on a Euro EA 3000 Elemental Analyzer. IR spectra were obtained on a Perkin-Elmer 577 spectrometer and recorded from 4000 to 450 cm^{-1} as a Nujol mull on KBr plates. ^1H NMR spectra were recorded on a Bruker DPX 200 NMR spectrometer, operating at 200 MHz. Chemical

*To whom correspondence should be addressed. Phone: +7-831-4354021. Fax: +7-831-4627497. E-mail: mboch@iomc.ras.ru.

(1) *Highly Efficient OLEDs with Phosphorescent Materials*; Yersin, H., Ed.; Wiley-VCH: Weinheim, Germany, 2008.
(2) (a) D'Andrade, B. W.; Forrest, S. R. *Adv. Mater.* **2004**, *16*, 1585–1595. (b) Evans, R. C.; Douglas, P.; Winscom, C. J. *Coord. Chem. Rev.* **2006**, *250*, 2093–2126. (c) Chou, P. T.; Chi, Y. *Chem.—Eur. J.* **2007**, *13*, 380–395. (d) De Bettencourt-Dias, A. *Dalton. Trans.* **2007**, 2229–2241. (e) Katkova, M. A.; Vitukhnovsky, A. G.; Bochkarev, M. N. *Russ. Chem. Rev.* **2005**, *74*, 1089–1109. (f) Binnemans, K. *Chem. Rev.* **2009**, *109*, 4283–4374.
(3) (a) Kido, J.; Okamoto, Y. *Chem. Rev.* **2002**, *102*, 2357–2368. (b) Bochkarev, M. N.; Katkova, M. A. In *Handbook of Light Emitting and Schottky Diode Research*; Chen, N. P., Ed.; Nova Science Publishers, Inc: New York, 2009; pp 1−65.
(4) Burrows, P. E.; Sapochak, L. S.; McCatty, D. M.; Forrest, S. R.; Thompson, M. E. *Appl. Phys. Lett.* **1994**, *64*, 2718–2720.
(5) Katkova, M. A.; Ilichev, V. A.; Konev, A. N.; Bochkarev, M. N.; Vitukhnovsky, A. G.; Parshin, M.; Pandey, L.; Van der Auweraer, M. *J. Appl. Phys.* **2008**, *104*, 053706–053706(3).
(6) Bradley, D. C.; Chotra, J. S.; Hart, F. A. *J. Chem. Soc., Dalton Trans.* **1973**, 1021–1023.

Published on Web 04/27/2010

shifts were given in parts per million and referenced to tetramethylsilane, $SiMe_4$. The HOMO energies for scandium complexes **1**−**3** were determined by photoelectron spectroscopy, using a NANOFAB 25 (NT-MDT Co., Zelenograd, Moscow, Russia) photoelectron spectrometer.

Synthesis of $Sc(C_{13}H_9N_2O)_3$ (1). A solution of 2-(2-hydroxyphenyl)-1H-benzimidazole (278 mg, 1.32 mmol) in DME (10 mL) was added to a solution of $Sc[N(SiMe_3)_2]_3$ (283 mg, 0.44 mmol) in DME (5 mL). The reaction mixture was stirred for 30 min at room temperature, and the solvent was evaporated under a vacuum. The solid residue was washed with toluene and dried under a vacuum to give **1** as a beige powder. Yield: 281 mg, 95%. Anal. Calcd for $C_{39}H_{27}N_6O_3Sc$: C, 69.64; H, 4.05; N, 12.49; Sc, 6.68. Found: C, 69.69; H, 4.15; N, 12.43; Sc, 6.62. IR (Nujol, cm^{-1}): 3170 (w), 3050 (br), 1623 (m), 1600 (m), 1560 (m), 1527 (m), 1311 (m), 1265 (m), 1130 (w), 1038 (w), 965 (w), 915 (w), 850 (s), 803 (m), 738 (s), 615 (m). ^{1}H NMR (200 MHz, Py-d_5): δ 6.70−6.80 (m, 2H, C_{Ar}−H), 7.06−7.34 (m, C_{Ar}−H), 8.13−8.20 (m, 2H, C_{Ar}−H), 8.60 (d, 1H, C_{Ar}−H), 13.2 (1H, NH).

Synthesis of $Sc(C_{13}H_8NO_2)_3$ (2). The compound was prepared similarly to **1** from $Sc[N(SiMe_3)_2]_3$ (283 mg, 0.44 mmol) and 2-(2-hydroxyphenyl)benzoxazole (279 mg, 1.32 mmol). Yield: 273 mg, 92%. Anal. Calcd for $C_{39}H_{24}N_3O_6Sc$: C, 69.34; H, 3.58; N, 6.22; Sc, 6.65. Found: C, 69.39; H, 3.62; N, 6.26; Sc, 6.71. IR (Nujol, cm^{-1}): 3050 (br), 1607 (m), 1558 (w), 1523 (m), 1331 (w), 1284 (w), 1257 (m), 1155 (w), 1057 (w), 869 (m), 802 (m), 740 (s), 615 (m). ^{1}H NMR (200 MHz, Py-d_5): δ 6.68 (d, 1H, C(6)−H), 6.85 (t, 1H, C(4)−H), 6.98−7.76 (m, C_{Ar}−H), 7.97−8.02 (m, 2H, C_{Ar}−H).

Synthesis of $Sc(C_{13}H_8NSO)_3$ (3). The compound was prepared similarly to **1** from $Sc[N(SiMe_3)_2]_3$ (283 mg, 0.44 mmol) and 2-(2-hydroxyphenyl)benzothiazole (300 mg, 1.32 mmol). Yield: 296 mg, 93%. Anal. Calcd for $C_{39}H_{24}N_3O_3S_3Sc$: C, 64.72; H, 3.34; N, 5.81; S, 13.29; Sc, 6.21. Found: C, 64.78; H, 3.41; N, 5.89; S, 13.33; Sc, 6.27. IR (Nujol, cm^{-1}): 3050 (br), 1597 (s), 1554 (m), 1335 (m), 1318 (m), 1263 (w), 1216 (w), 1156 (w), 970 (w), 878 (m), 842 (m), 750 (s), 724 (s), 616 (m). ^{1}H NMR (200 MHz, Py-d_5): δ 6.99 (t, 1H, C(4)−H), 7.28−7.49 (m, C_{Ar}−H), 8.02−8.10 (m, 2H, C_{Ar}−H).

X-Ray Crystallographic Studies of 1 and 2. The X-ray diffraction data were collected on a SMART APEX diffractometer (graphite-monochromated, Mo Kα radiation, φ−ω-scan technique, λ = 0.71073 Å). The intensity data were integrated by the SAINT program.[7] SADABS[8] was used to perform area-detector scaling and absorption corrections. The structures were solved by direct methods and were refined on F^2 using all reflections with the SHELXTL package.[9] All non-hydrogen atoms were refined anisotropically. H atoms in **1**$(THF)_2$ were found from Fourier synthesis and refined isotropically except for the H atoms of the disordered THF molecule, which were placed in calculated positions and refined in the "riding model". H atoms in **2** were placed in calculated positions and refined in the "riding model". Details of crystallographic, collection and refinement data for **1** and **2** are shown in the Table 1.

Computational Details. To investigate the electronic structures of **1**, **2**, and **3** and to interpret differences in their electroluminescent properties, DFT calculations of the complexes' level have been performed with the use of the Gaussian 03 package.[10] Generalized gradient approximation (GGA) functional BPW91[11] was employed in combination with the triple-ζ valence quality TZVP basis set.[12] The geometries of the lowest singlet (S_0) electronic state were fully optimized. The absence of imaginary frequencies testified for the energy minimum. To explain the trends in the electroluminescence of **1**, **2**, and **3**, their HOMO and LUMO energies were compared.

Device Fabrication. OLED devices were prepared in a vacuum system with different resistive heaters for different types of organic and metal layers.[13] The simple nondoped two-layer devices ITO/TPD/Sc complex/Yb, consisting of a triphenyldiamine derivative (TPD) as a hole transport layer and scandium chelated heterocyclic complex as an electron transport and emission layer, were fabricated. A commercial ITO on a glass substrate with 100 Ω/sq. was used as the anode material (Merck Balzers) and commercial Yb, 99.9% trace metals basis (Sigma-Aldrich), as the cathode material.[13] The constituent organic (25 nm) and metal (150 nm) layers were deposited using thermal vacuum deposition (at a base pressure of approximately 10^{-6} mbar) of commercial grade TPD and Yb metal and freshly synthesized scandium complexes **1**, **2**, and **3**. The active area of the devices was a circle with ∅ 5 mm. The EL spectra and current−voltage luminescence characteristics were measured with an Ocean Optics USB-2000 fluorimeter and a computer controlled TEC-23 power supply under ambient conditions.

Results and Discussion

Synthesis of 1−3. It is known that the rare earth complexes synthesized by the traditional water−alcohol method, as a rule, contain coordinated water or acid residuals, which greatly impair their luminescent properties and make them of little avail for the design of OLEDs. To avoid this drawback in our previous works, we did use a traditional organometallic chemistry method based on the chemical reactions of rare earth silylamides with the substrates containing a labile hydrogen atom such as alcohols, thiols, or selenols yielding the respective derivatives of the $Ln(XR)_3$ type.[14] This method

(7) *SAINTPlus Data Reduction and Correction Program*, v. 6.02a; Bruker AXS: Madison, WI, 2000.

(8) Sheldrick, G. M. *SADABS*, v.2.01, Bruker/Siemens Area Detector Absorption Correction Program; Bruker AXS: Madison, WI, 1998.

(9) Sheldrick, G. M. *SHELXTL*, v. 6.12, Structure Determination Software Suite; Bruker AXS: Madison, WI, 2000.

(10) Frisch, M. J.; Trucks, G. W.; Schlegel, H. B.; Scuseria, G. E.; Robb, M. A.; Cheeseman, J. R.; Montgomery, J. A., Jr.; Vreven, T.; Kudin, K. N.; Burant, J. C.; Millam, J. M.; Iyengar, S. S.; Tomasi, J.; Barone, V.; Mennucci, B.; Cossi, M.; Scalmani, G.; Rega, N.; Petersson, G. A.; Nakatsuji, H.; Hada, M.; Ehara, M.; Toyota, K.; Fukuda, R.; Hasegawa, J.; Ishida, M.; Nakajima, T.; Honda, Y.; Kitao, O.; Nakai, H.; Klene, M.; Li, X.; Knox, J. E.; Hratchian, H. P.; Cross, J. B.; Adamo, C.; Jaramillo, J.; Gomperts, R.; Stratmann, R. E.; Yazyev, O.; Austin, A. J.; Cammi, R.; Pomelli, C.; Ochterski, J. W.; Ayala, P. Y.; Morokuma, K.; Voth, G. A.; Salvador, P.; Dannenberg, J. J.; Zakrzewski, V. G.; Dapprich, S.; Daniels, A. D.; Strain, M. C.; Farkas, O.; Malick, D. K.; Rabuck, A. D.; Raghavachari, K.; Foresman, J. B.; Ortiz, J. V.; Cui, Q.; Baboul, A. G.; Clifford, S.; Cioslowski, J.; Stefanov, B. B.; Liu, G.; Liashenko, A.; Piskorz, P.; Komaromi, I.; Martin, R. L.; Fox, D. J.; Keith, T.; Al Laham, M. A.; Peng, C. Y.; Nanayakkara, A.; Challacombe, M.; Gill, P. M. W.; Johnson, B.; Chen, W.; Wong, M. W.; Gonzalez, C.; Pople, J. A. *Gaussian 03*; Gaussian, Inc.: Pittsburgh, PA, 2003.

(11) (a) Becke, A. D. *Phys. Rev. A* **1988**, *38*, 3098–3100. (b) Perdew, J. P.; Burke, K.; Wang, Y. *Phys. Rev. B* **1996**, *54*, 16533–16539.

(12) (a) Schaefer, A.; Horn, H.; Ahlrichs, R. *J. Chem. Phys.* **1992**, *97*, 2571–2577. (b) Schaefer, A.; Huber, C.; Ahlrichs, R. *J. Chem. Phys.* **1994**, *100*, 5829–5835.

(13) (a) Katkova, M. A.; Ilichev, V. A.; Konev, A. N.; Batenkin, M. A.; Pestova, I. I.; Vitukhnovsky, A. G.; Bochkarev, M. N. *Appl. Surf. Sci.* **2008**, *254*, 2216–2219. (b) Bochkarev, M. N.; Katkova, M. A.; Ilichev, V. A.; Konev, A. N. *Nanotechnol. Russia* **2008**, *3*, 470–473. (c) Ilichev, V. A.; Katkova, M. A.; Konev, A. N.; Pestova, I. I.; Bochkarev, M. N. *Proceedings of the 27th International Display Research Conference*, **2007**; pp 396−399.

(14) (a) Katkova, M. A.; Kurskii, Y. A.; Fukin, G. K.; Averyushkin, A. S.; Artamonov, A. N.; Vitukhnovsky, A. G.; Bochkarev, M. N. *Inorg. Chim. Acta* **2005**, *358*, 3625–3632. (b) Katkova, M. A.; Borisov, A. V.; Fukin, G. K.; Baranov, E. V.; Averyushkin, A. S.; Vitukhnovsky, A. G.; Bochkarev, M. N. *Inorg. Chim. Acta* **2006**, *359*, 4289–4296. (c) Katkova, M. A.; Ilichev, V. A.; Konev, A. N.; Pestova, I. I.; Fukin, G. K.; Bochkarev, M. N. *Org. Electron.* **2009**, *10*, 623–630. (d) Ilichev, V. A.; Katkova, M. A.; Konev, A. N.; Bochkarev, M. N. *Polyhedron* **2010**, *29*, 400–404.

Table 1. X-ray Data Collection Parameters for Complexes **1** and **2**

	1(THF)$_2$	**2**
empirical formula	$C_{47}H_{43}N_6O_5Sc$	$C_{39}H_{24}N_3O_6Sc$
fw	816.83	675.57
temp (K)	100(2)	100(2)
wavelength (Å)	0.71073	0.71073
cryst syst, space group	triclinic, $P\bar{1}$	monoclinic, $P2_1/c$
unit cell dimensions		
a (Å)	9.3688(5)	9.9164(4)
b (Å)	10.6914(6)	18.7888(8)
c (Å)	20.7119(11)	16.3723(7)
α (deg)	90.175(1)	90
β (deg)	93.060(1)	93.1060(10)
γ (deg)	109.645(1)	90
volume (Å^3)	1950.59(18)	3046.0(2)
Z, calcd density (Mg/m^3)	2, 1.391	4, 1.473
absorption coeff (mm^{-1})	0.247	0.299
F(000)	856	1392
cryst size (mm)	0.32 × 0.15 × 0.07	0.36 × 0.22 × 0.18
θ range for data collection (deg)	2.31−26.00	2.06−26.00
limiting indices	$-11 \le h \le 11$, $-13 \le k \le 13$, $-25 \le l \le 25$	$-12 \le h \le 12$, $-23 \le k \le 23$, $-20 \le l \le 20$
reflns collected/unique [R_{int}]	17152/7648 [0.0665]	25870/5967 [0.0412]
completeness to θ = 26.50	99.5%	99.7%
absorption correction	semiempirical from equivalents	semiempirical from equivalents
max. and min transmission	0.9829 and 0.9252	0.9481 and 0.9000
refinement method	full-matrix least-squares on F^2	full-matrix least-squares on F^2
data/restraints/params	7648/18/697	5967/0/442
goodness-of-fit on F^2	0.976	1.064
final R indices [$I > 2\sigma(I)$]	R_1 = 0.0558, wR_2 = 0.1047	R_1 = 0.0578, wR_2 = 0.1423
R indices (all data)	R_1 = 0.1035, wR_2 = 0.1145	R_1 = 0.0776, wR_2 = 0.1522
largest diff. peak and hole (eÅ^{-3})	0.681 and −0.393	1.525 and −0.611

Table 2. Thin Films Absorption and Emission Data for Complexes **1**−**3**

complex	λ_{maxAbs} (nm)	λ_{maxEx} (nm)	λ_{maxEm} (nm)
1	295, 345	375	430
2	295, 360	370	440
3	295, 365	375	455

affords neutral mononuclear water- and acid-residual-free compounds in high yield. Herein, we have spread this convenient synthesis pathway to complexes **1**−**3**. The desired products were prepared in quantitative yield from Sc[N(SiMe$_3$)$_2$]$_3$ and corresponding heterocyclic phenol.

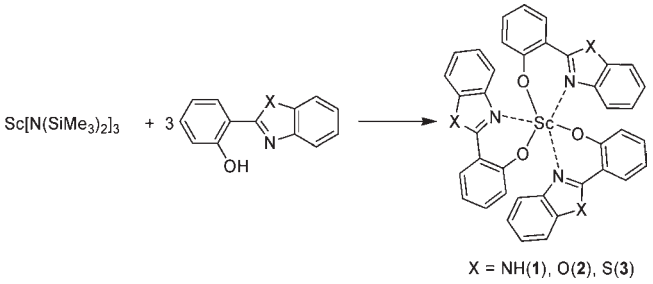

All of the new scandium complexes are beige crystalline solids which can be sublimed in a vacuum without decomposition. Their tolerable stability in air allows the use of them without any special precautions. They are found to form smooth and uniform films by vacuum deposition. Table 2 illustrates their absorption and photoluminescent data recorded from vacuum-deposited thin films.

Crystal Structures of 1 and 2. The suitable crystals of **1** and **2** for X-ray analysis were obtained by very slow evaporation of a THF solution for 5 days. The X-ray investigation revealed that the Sc atom in these compounds is coordinated by three bidentate ligands via the

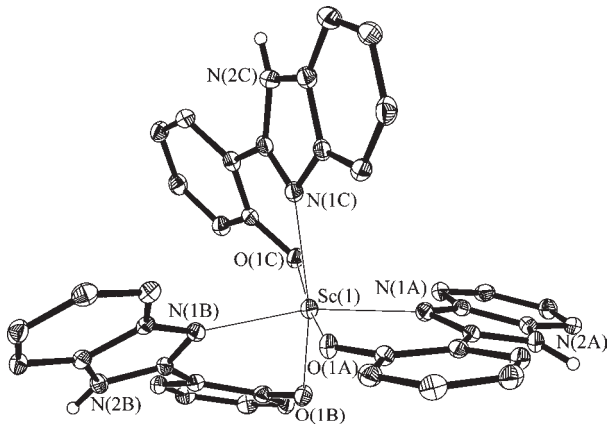

Figure 1. Molecular structure of **1**. Table 3 contains selected bond lengths [Å] and angles [deg]. Anisotropic displacement parameters are drawn at the 30% probability level. H atoms (except for those of N2) and THF solvent molecule are omitted for clarity.

azole N and phenoxy O atoms and located in a distorted octahedral geometry (Figures 1 and 2). The use of fac-mer approaches for the description of isomers has shown that both complexes are *fac* isomers. The Sc−O and Sc−N distances in a molecule of **1** (1.986(1)−2.055(1) Å and 2.246(1)−2.373(1) Å, respectively) are close to corresponding bond lengths in **2** (1.992(2)−2.004(2) Å and 2.275(2)−2.348(2) Å) (Table 3). This fact shows the negligible influence of variation of the heteroatoms (NH and O) of the heterocyclic ring on these bonds. On the other hand, the dihedral angles between the phenolate and heterocycle moieties in **1** are 14.1° for ligand **A**, 31.7° for **B**, and 26.9° for **C**, whereas the corresponding ligands in **2** have a basically planar fashion. Such significant deviation of ligand planarity can be explained by different

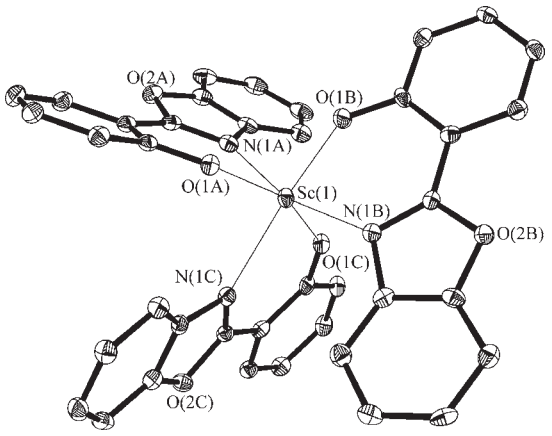

Figure 2. Molecular structure of **2**. Table 3 contains selected bond lengths [Å] and angles [deg]. Anisotropic displacement parameters are drawn at the 30% probability level. H atoms are omitted for clarity.

Table 3. Selected Bond Lengths [Å] and Angles [deg] of **1**, **2**, and **3**

	X-ray analysis		DFT calculation		
	1(THF)$_2$	**2**	**1**	**2**	**3**
		Distances			
Sc(1)−N(1A)	2.254(2)	2.275(2)	2.344	2.336	2.371
Sc(1)−N(1B)	2.246(1)	2.341(2)	2.345	2.341	2.372
Sc(1)−N(1C)	2.373(1)	2.348(2)	2.409	2.430	2.450
Sc(1)−O(1A)	1.986(1)	2.004(2)	2.031	2.025	2.014
Sc(1)−O(1B)	2.055(1)	1.992(2)	2.015	2.000	2.013
Sc(1)−O(1C)	2.021(1)	2.004(2)	2.023	2.030	2.012
		Angles			
O(1A)Sc(1)N(1A)	80.39(5)	79.30(8)	78.40	79.0	76.58
O(1B)Sc(1)N(1B)	80.56(5)	79.42(8)	79.23	79.35	78.09
O(1C)Sc(1)N(1C)	77.57(5)	77.75(8)	76.94	76.58	77.74
O(1B)Sc(1)O(1C)	88.61(5)	100.48(8)	96.42	94.18	97.57
O(1A)Sc(1)O(1B)	102.23(5)	99.81(8)	98.85	99.67	105.14
O(1A)Sc(1)O(1C)	169.02(5)	153.82(8)	162.21	165.56	153.13
N(1B)Sc(1)N(1C)	91.55(5)	96.29(8)	93.06	95.16	92.18
N(1A)Sc(1)N(1C)	98.77(5)	99.82(8)	97.45	95.49	99.99
N(1B)Sc(1)N(1A)	166.04(6)	163.64(8)	167.25	167.55	166.97

intermolecular interactions involving hydrogen bonding and/or stacking interactions. In **1**, the imidazole group donates a hydrogen bond to the O atom of a solvent THF molecule with a corresponding O(1S)−H distance of 1.90 Å. In addition, there are intermolecular contacts between O···H (2.41 Å) atoms of imidazole and phenolate moieties.

A $\pi-\pi$ stacking interaction offset type for **1** and face to face type for **2** describe the arrangement of molecules in the crystals of both complexes. The interaction occurs between the heterocyclic moieties of adjacent ligands as shown in Figures 3 and 4. The shortest intermolecular distances are 3.412 Å for **1** and 3.357 Å for **2**, which close to 3.35 Å between the layers of graphite. These peculiarities in the crystal structures suggest that complexes **1** and **2** could possess good carrier transport properties.

DFT. To check whether the ligand distortions in **1** are caused by intermolecular interactions or whether they can take place in a free molecule and to predict a molecular structure of **3**, geometry optimizations of **1**−**3** have been performed. The optimized geometries of **1**, **2**, and **3** are given in Figure 5. The interatomic distances and angles of

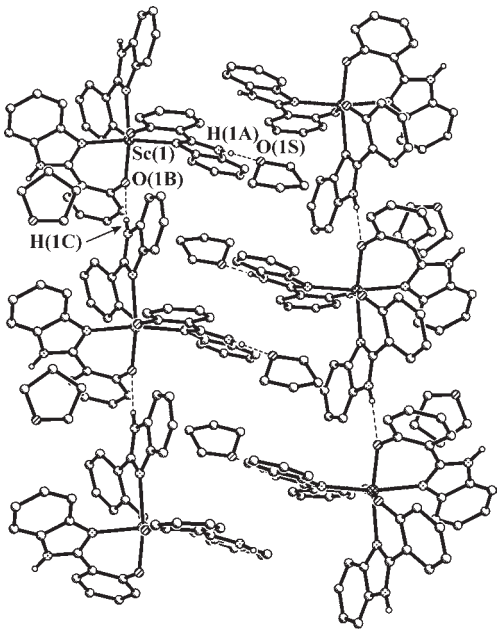

Figure 3. Fragment of crystal packing of **1(THF)$_2$**.

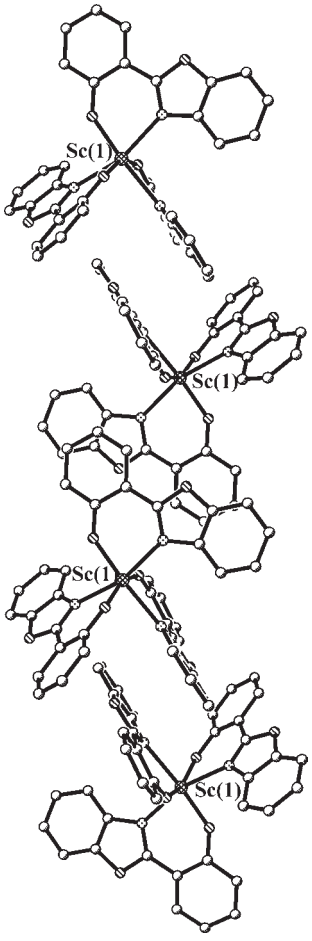

Figure 4. Fragment of crystal packing of **2**.

the optimized **1**−**3** molecules are compared with those determined from X-ray analysis in Table 3. The X-ray experiment and the DFT calculation reveal similar trends for the metal−ligand bond lenghts. The O and N atoms in

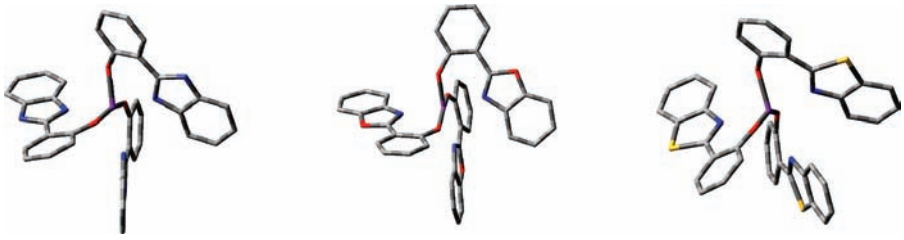

Figure 5. Optimized (BPW91/TZVP) geometries of the **1**, **2**, and **3** molecules. The hydrogen atoms are omitted for clarity.

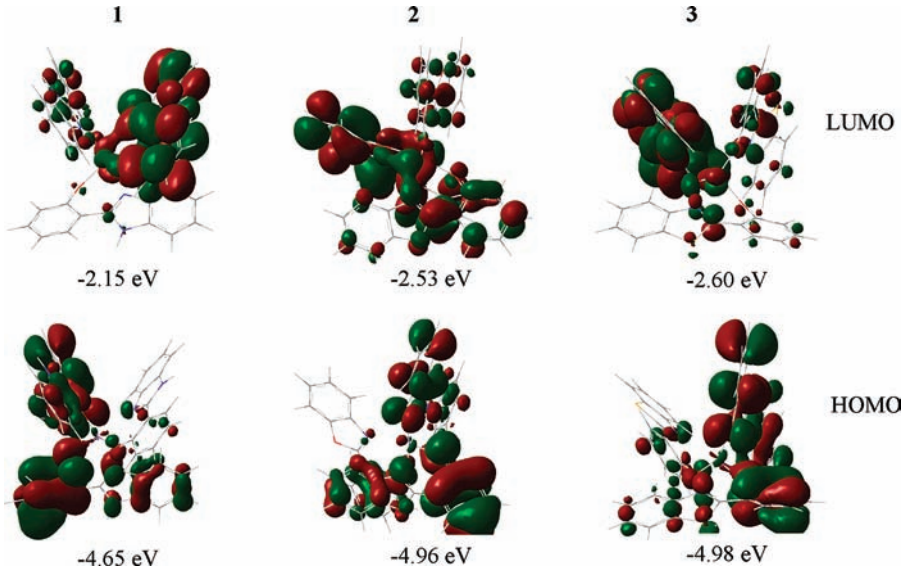

Figure 6. The HOMO and LUMO isosurfaces (the electron density of 0.02 a.u.) for complexes **1**−**3**.

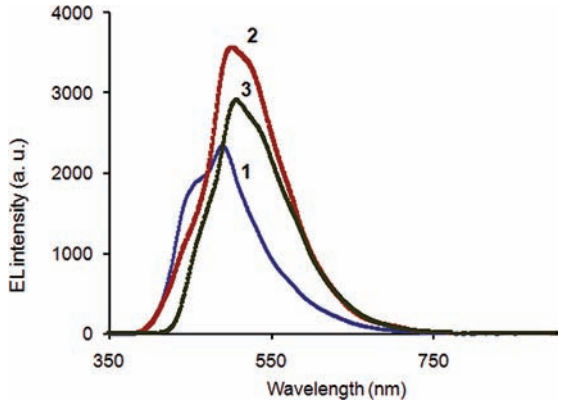

Figure 7. EL spectra of single layer devices ITO/**1**/Yb (1), ITO/**2**/Yb (2), and ITO/**3**/Yb (3).

1−**3** form two T-shaped triads within the distorted octahedral eviroment of the metal atom. Each triad can be considered a combination of two "axial" atoms with the O−Sc−O or N−Sc−N bond angle close to 160° (O(1A) and O(1C) or N(1A) and N(1B)) and an atom belonging to an equatorial plane and forming an O−Sc−O or N−Sc−N angle close to 90° (O(1B) or N(1C)). Both the X-ray experiment and the calculation reveal an increase in the Sc−N bond length on going from the "axial" to the "equatorial" nitrogen atom. There is no such a trend for the Sc−O bonds (Table 3). According to the computational results, the ligands in the free molecule of **1** are less distorted from the planar configuration than those in the

Chart 1

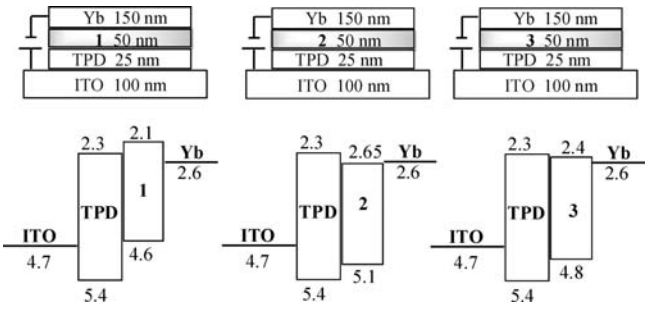

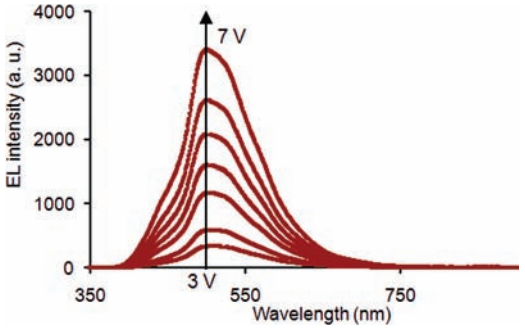

Figure 8. The EL spectra of the device ITO/TPD/**2**/Yb at different applied voltages.

crystal structure. However, the dihedral angle between the phenolate and heterocyclic planes in the **B** ligand of

the **1** molecule is calculated to be 20.0°. This indicates that the ligand distortion can be caused not only by the intermolecular interactions but also by the intramolecular forces. Similar to the X-ray experiment, DFT shows that the ligands in **2** are almost planar. The calculation allows us to predict the molecular structure of **3** (Figure 5).

On going from **1** and **2** to **3**, the angle between the Sc−O bonds for the "axial" oxygen atoms decreases by ∼10°. Simultaneously the O(1A)−Sc−O(1B) angle increases to 105.14° (Table 3). The bond lengths change little when one goes from **2** to **3**. However, the ligand orientation in the **3** molecule appears to be different from that in **2**. In complex **2**, the Sc atom lies very close (0.07 A) to the plane formed by three O atoms bounded to the metal. On going to **3**, this distance increases to 0.21 A. The **B** ligand in **2** is nearly coplanar with the O(1A)−O(1B)−O(1C) plane, while in the **3** molecule the corresponding ligand is rotated and its sulfur-containing fragment forms an angle of 37.7° with the oxygen plane (Figure 5). These differences in the complex geometries can be responsible for the difficulties in crystallization of compound **3** as well as for changes in electroluminescence on going from **2** to **3**. On the other hand, the efficiency of light emission by **1**−**3** should depend on the properties of the frontier molecular orbitals of the complexes.

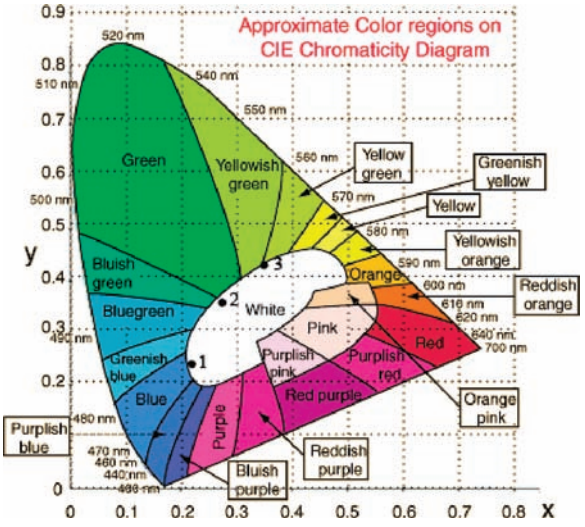

Figure 9. Emission colors of two-layer devices based on **1**, **2**, and **3** in a CIE chromaticity diagram.

The HOMO of **1**, **2**, and **3** represents an almost pure ligand orbital with a metal contribution of less than 1%. On going to LUMO, the contribution of the metal wave functions increases to 26, 22, and 14% for **1**−**3**, respectively. It should be noted that the electron density distribution between the ligands is different for the HOMO and the LUMO. The orbital shapes are given in Figure 6. The HOMO−LUMO electronic transition can be considered, therefore, as an interligand charge transfer with a contribution of LMCT. The HOMO energy decreases as **1** (−4.65 eV) > **2** (−4.96 eV) > **3** (−4.98 eV). The same trend is observed for the LUMO energy (−2.15,

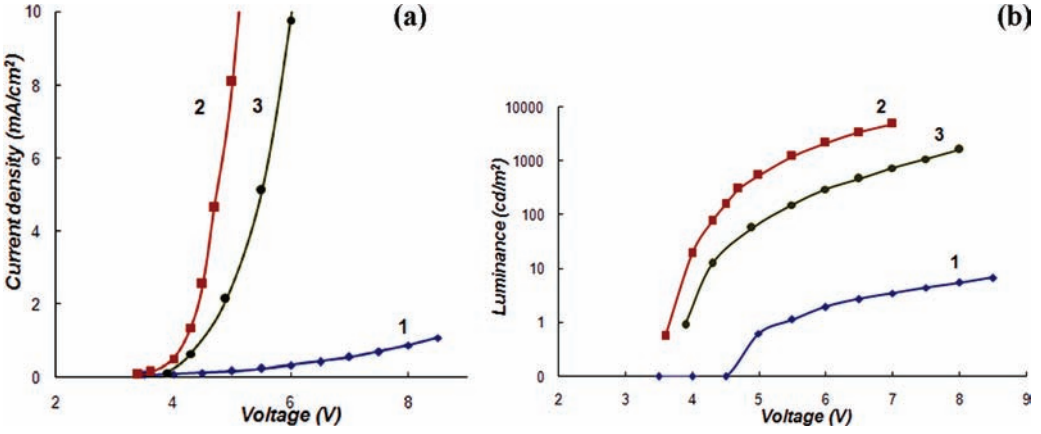

Figure 10. Current density (a) and luminance (b) as a function of operating voltage for OLED devices ITO/TPD/**1**/Yb (1), ITO/TPD/**2**/Yb (2), and ITO/TPD/**3**/Yb (3).

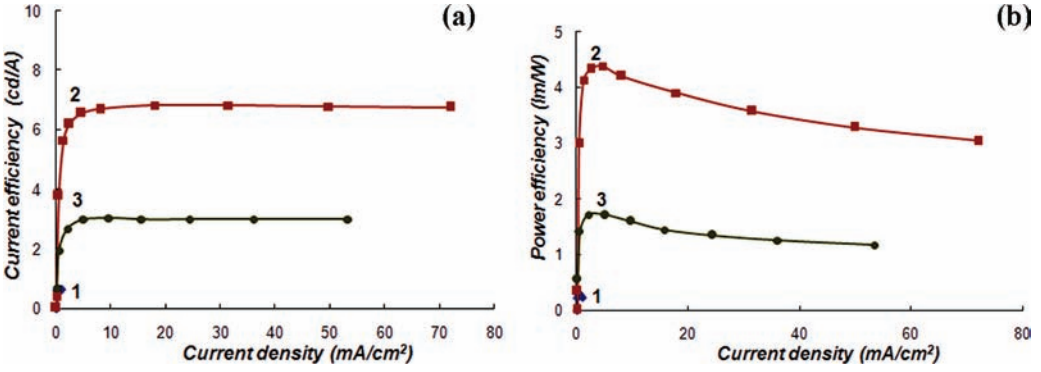

Figure 11. Current efficiency (a) and power efficiency (b) vs current density for OLED devices ITO/TPD/**1**/Yb (1), ITO/TPD/**2**/Yb (2), and ITO/TPD/**3**/Yb (3).

Table 4. Performance Characteristics for the Two-Layer Devices Based on Scandium Complexes **1**, **2**, and **3**

scandium complex	turn-on voltage (V)	current efficiency (cd/A)	power efficiency (lm/W)	driving voltage (V)	CIE(x; y)
1	4.8	0.6	0.3	7.0	0.2147; 0.2379
2	3.0	6.2	4.3	4.5	0.2702; 0.3524
3	4.5	3.0	1.7	5.5	0.3468; 0.4284

−2.53, and −2.60 eV for **1**, **2**, and **3**, respectively). The higher energies of the **1** frontier orbitals can result in different electroluminiscent properties of complex **1** as compared to compounds **2** and **3**.

Electroluminescent Properties. The simple single layer devices on a base of obtained Sc compounds revealed an emission as a broad band in a range of 450−550 nm with low efficiency (Figure 7). The light output in all the cases did not exceed 10 cd/m^2.

To improve the performances of these OLEDs, the following bilayer devices of ITO/TPD/**1**/Yb, ITO/TPD/**2**/Yb, and ITO/TPD/**3**/Yb were fabricated where TPD was chosen as a standard hole transporting layer material for small-molecule-based OLEDs. The schematic device architecture and the estimated energy-level diagram are depicted in Chart 1. The HOMO energies for **1**, **2**, and **3** were determined by photoelectron spectroscopy with a He I UV source that has a photon energy of 21.2 eV. The LUMO energies were determined using the HOMO energies and the optical band gaps estimated from the absorption spectra.

The EL spectra of these devices resembled the spectra of corresponding single-layer devices, and as shown for **2** (Figure 8), they did not significantly change with variation of the operating bias voltages.

As a general trend, the emission peak slightly shifts to longer wavelengths from **1** through **2** to **3**, correlating with the decrease in the LUMO−HOMO energy gap (2.50, 2.45, and 2.4 eV for **1**−**3**, respectively). At the same time, the EL characteristics of these devices are significantly different. To the naked eye, the emission from the device based on **1** appeared to be close to near-white with a blue hue; **2** had a cyan hue, and **3** had a yellowish hue. CIE coordinates are shown in Figure 9 (CIE = Commission Internationale de L'Eclairage; the ideal white is $x = 0.33$, $y = 0.33$). Figure 10 displays the current−voltage (a) and luminance−voltage (b) characteristics for the two-layer devices. Figure 11 shows the current efficiency (cd/A) (a) and the power efficiency (lm/W) (b) vs the current density. The basic characteristics and performance data are summarized in Table 4.

The device based on **2** reveals noticeably better characteristics than the devices with **1** and **3**: both the $J-V$ and $L-V$ curves in the case of **2** shift to lower driving voltage; the turn-on voltage (to obtain a current density of 0.1 mA/cm^2) for **2** (3.0 V) is also lower than the value for the devices with **1** (4.8 V) and **2** (4.5 V) layers. A maximum luminance of 4867 cd/m^2 and a maximum emission efficiency of 6.2 cd/A for **2** are highest among these devices. In contrast, the luminance and emission efficiency of the device based on **1** were significantly inferior to those of the device based on **2** and **3**. This can be a result of the higher LUMO energy of **1** as compared to that of **2** and **3**. Hereby, although the studied EL devices have not been optimized, their high performance characteristics give the basis to expect that the scandium complexes as emissive materials would have a significant impact on the development of OLEDs.

Conclusions

In summary, we report the synthesis and X-ray structural characterization of some new scandium chelated heterocyclic complexes and their applications in two-layer OLED devices. In contrast to the most frequently applied dual or multiple dopants in multilayer white OLED devices, all our simpler devices with a neat emissive layer based on **1**−**3** exhibit bright close to near-white light with a blue hue (CIE$_{x,y}$ = 0.2147, 0.2379) in the case of **1**, a cyan hue (0.2702, 0.3524) in the case of **2**, and yellowish hue (0.3468, 0.4284) in the case of **3**.

Acknowledgment. This work was supported by the Russian Foundation of Basic Research (Grants, 10-03-00190, 09-03-97016p, 09-03-97045p, 08-03-97054p) and the Russian Federal Agency for Education (Federal program "Scientific and pedagogical professionals of innovative Russia," Contract P337). The authors express their gratitude to Vice-rector Professor Drs. S.E. Alexandrov and Dr A.L. Shakhmin, from St. Petersburg State Polytechnic University, for UPS measurements.

Note Added after ASAP Publication. This paper was published ASAP on April 27, 2010, without the term "close to" in correspondence with "near-white" throughout the text. The corrected version was published on May 4, 2010.

Supporting Information Available: X-ray crystallographic data of complex **1** and **2** in CIF format. This material is available free of charge via the Internet at http://pubs.acs.org.